INL/EXT-21-64733 Rev. 001

Multiscale Modeling of Cr_2O_3-doped UO_2 Creep and Fracture

30 August 2022

Technical Report

Kyle A. Gamble[1] and Michael W. D. Cooper[2]

[1]Idaho National Laboratory
[2]Los Alamos National Laboratory

INL is a U.S. Department of Energy National Laboratory
operated by Batelle Energy Alliance, LLC

Multiscale Modeling of Cr_2O_3-doped UO_2 Creep and Fracture

Technical Report

Kyle A. Gamble[1] and Michael W. D. Cooper[2]

[1]Idaho National Laboratory
[2]Los Alamos National Laboratory

30 August 2022

Idaho National Laboratory
Computational Mechanics and Materials Department
Idaho Falls, Idaho 83415

http://www.inl.gov

Prepared for the
U.S. Department of Energy
Office of Nuclear Energy
Under U.S. Department of Energy-Idaho Operations Office
Contract DE-AC07-05ID14517

Page intentionally left blank

Abstract

The pursuit of UO_2 fuel with various dopants (e.g., Cr_2O_3 and Al_2O_3) for improved accident tolerance due to larger grain sizes and suspected reductions in fission gas release and creep requires advanced modeling and simulation tools. Such tools enable rapid multiscale development and enhanced understanding of material behavior in regimes for which experimental measurements may be lacking.

This work builds on previous multiscale modeling efforts targeting the fission gas behavior of Cr_2O_3-doped UO_2, in order to begin exploring the effects of dopants on mechanical properties, with a particular focus on creep and fracture. The results indicate that dislocation climb is the most dominate creep mechanism at almost all temperatures, and sensitivity analyses provide evidence in further support of this claim.

The limited experimental data generated by the U.S. Department of Energy's Advanced Fuels Campaign (AFC) on the tensile strength of Cr_2O_3-doped UO_2 indicate that fracture may be less severe in doped specimens. The results on creep and fracture are preliminary, given the large degree of uncertainty associated with the models.

Page intentionally left blank

Acknowledgments

This report was authored by a contractor of the U.S. Government under Contract DE-AC07-05ID14517. Accordingly, the U.S. Government retains a non-exclusive, royalty-free license to publish or reproduce the published form of this report, or allow others to do so, for U.S. Government purposes.

Contributions have been provided by Los Alamos National Laboratory, an affirmative action/equal opportunity employer operated by Triad National Security, LLC, for the National Nuclear Security Administration of the U.S. Department of Energy under Contract No. 89233218CNA000001.

This research made use of the resources of the High Performance Computing Center at Idaho National Laboratory, which is supported by the Office of Nuclear Energy of the U.S. Department of Energy and the Nuclear Science User Facilities under Contract No. DE-AC07-05ID14517.

Page intentionally left blank

Contents

List of Figures

List of Tables

Acronyms

AFC	Advanced Fuels Campaign
ATF	accident-tolerant fuel
LANL	Los Alamos National Laboratory
LHGR	linear heat generation rate
LWR	light-water reactor

1. Introduction

Doped UO_2 fuel concepts are being actively investigated for enhancing the accident tolerance of light-water reactors (LWRs). The primary dopants of interest include the fine ceramic compounds of Cr_2O_3 and Al_2O_3. The main benefit identified from including these dopants is increased grain size, which potentially reduces the amount of fission gas release into the plenum. Recent work by Cooper et al. [1] utilized a multiscale modeling approach to show that the diffusion coefficients of fission gases (e.g., Xe) are larger in Cr_2O_3-doped UO_2. Utilization of lower length scale modeling to inform the diffusion coefficients used at the engineering scale improved predictions of fission gas release in Cr_2O_3-doped UO_2 experiments conducted at the Halden reactor in Norway.

As all primary LWR fuel vendors offer a doped UO_2 concept, the success of the multiscale modeling approach in regard to improving fission gas release modeling has fueled a desire for further multiscale modeling investigations in this area. Understanding the effect of dopants on creep- and fracture-related mechanical behavior is of particular interest, since these properties are usually a function of grain size.

This report introduces the preliminary multiscale modeling effort on creep and fracture in standard and doped UO_2 fuels. Next, it describes the preliminary creep model, then investigates the impact of that model on a sample problem, with sensitivity analysis included. After that, it discusses the different modeling techniques (and the applicability thereof) available in BISON [2] for modeling fracture. A brief discussion on collaborating with the Advanced Fuels Campaign (AFC) on tensile strength properties is also provided. The primary sections of the report end with a re-analysis of the IFA-677.1 rods 1 and 5 validation cases in the BISON validation database. The paper itself concludes with three sections pertaining to outcomes, future work, and a summary of this year's accident tolerant fuel-related publications by the authors of this report.

2. Preliminary Creep Model Development

Three creep mechanisms were considered in the development of the creep model: Nabarro-Herring, Coble, and climb-limited dislocation creep. The correlations obtained herein are applicable at 1123–2273 K and were derived from lower length scale data for typical LWR fission rates (10^{19} $m^{-3}s^{-1}$). The stress and grain size dependencies were captured by the mechanistic fits. The fact that grain size dependencies differ for each mechanism is important in terms of the applicability to large-grain doped UO_2. Unlike the MATPRO [3] correlation for creep, which is available in BISON [2], we include terms for both bulk (Nabarro-Herring) and grain boundary (Coble) diffusional creep. In all cases, a fourth-order polynomial, $f(t)$, was used to fit functions that described those creep rates that arose due to point defect diffusion processes while under irradiation and over a wide range of temperatures:

$$f\left(t\right) = At^4 + Bt^3 + Ct^2 + Dt + E \tag{2.1}$$

where $t = 10^4/T$, with T being the temperature in K.

The cluster dynamics data were taken from Centipede simulations of uranium self-diffusion under irradiation [4, 1], with contributions from a range of U defects. This forms the basis of the creep model described below.

2.1 Nabarro-Herring Creep

Nabarro-Herring creep occurs via the bulk diffusion of point defects in response to an applied strain. It arises due to the influence of stress on a defect's chemical potential. For example, the energy of vacancies is typically lower in a compressive strain field. Thus, under an applied stress, vacancies will diffuse from tensile to compressive regions, resulting in self-diffusion of U atoms in the opposite direction, such that mass is transported toward the tensile regions. This causes plastic deformation, which serves to relieve the stress (i.e., creep). The following equation approximates Nabarro-Herring creep [5, 6] caused by a given defect x:

$$\dot{\epsilon}_{NH,\ x} = \frac{42|\Omega_x|D_x[x]}{k_B T G^2}\sigma_v \tag{2.2}$$

where Ω_x is the defect volume; D_x and $[x]$ are the diffusivity and concentration of the defect, respectively; G is the grain size; σ_v is the von Mises stress; and k_B is the Boltzmann constant. In UO_2, diffusion on the oxygen sublattice is orders of magnitude faster than on the uranium sublattice. Therefore, for the system to deform in a stoichiometric manner, the creep rate is governed by defects on the uranium sublattice. Note that we still consider the binding of oxygen defects to uranium defects and the impact this has on their mobility. D_x and $[x]$ are taken from cluster dynamics simulations of UO_2 under irradiation using the Centipede code. It was found that the Nabarro-Herring creep rate was dominated by $\{U_i : 2O_i\}$ and V_U, where standard Kröger-Vink notation was used. At high temperatures, the point uranium vacancy (V_U) dominates, and at low temperatures, a uranium interstitial (U_i) bound to two oxygen interstitials (O_i) dominates. The dominance of the highly unstable $\{U_i : 2O_i\}$ defect at low temperatures is due to its irradiation-enhanced concentrations and its high mobility compared to uranium vacancies. Therefore, the total Nabarro-Herring creep rate is given by:

$$\dot{\epsilon}_{NH} = \dot{\epsilon}_{NH,V_U} + \dot{\epsilon}_{NH,\{U_i:2O_i\}} \tag{2.3}$$

where

$$\dot{\epsilon}_{NH} = \frac{\sigma}{G^2}\left[\exp\left(f_{\{u_i:2O_i\}}(t)\right) + \exp\left(f_{V_U}(t)\right)\right] \tag{2.4}$$

where σ is the von Mises stress in Pa and G is the grain size in m. The coefficients for the two polynomial functions ($f_{\{u_i:2O_i\}}(t)$ and $f_{V_U}(t)$) are described by Equation 2.1, as defined in Table 2.1.

2.2 Coble Creep

Diffusion of defects along grain boundaries results in Coble creep. In similar fashion to the Nabarro-Herring correlation described above, we also derived an expression for Coble creep, based on the point defect diffusivities from Centipede cluster dynamics simulations of self-diffusion. Ongoing atomic-scale work is being conducted under a separate milestone to directly evaluate the driving force and kinetics of defect diffusion along grain boundaries. This involves molecular dynamics simulations of the stability of grain boundary defects under an applied stress, in addition to the simulations of diffusion along the grain boundaries. Since that work is not yet complete, several approximations have been made. We assumed that the mobilities and relaxation volumes of defects at the grain boundaries are the same as those in the bulk, and that the concentrations of defects at the grain boundaries are six orders of magnitude greater than those in the bulk (this assumption was previously made with regard to grain boundary vacancy diffusion in BISON's physics-based fission gas model). Future lower length scale work will be crucial for relaxing these broad assumptions, and will significantly impact our estimates of Coble creep rates. The Coble creep rate due to defect x is given by [7]:

$$\dot{\epsilon}_{Coble,\ x} = \frac{42|\Omega_{x,GB}|[x_{GB}]D_{GB,x}\pi\delta}{k_B T G^3}\sigma_v \tag{2.5}$$

where $D_{GB,x}$ is the grain boundary diffusivity of a given defect and is taken to be the same as the bulk diffusivity, D_x. The grain boundary concentration of a given defect, $[x_{GB}]$, is assumed to be six orders of

magnitude greater than the thermal equilibrium bulk concentration. $\Omega_{x,GB}$ is the defect volume at the grain boundary and is assumed to be identical to the bulk value, Ω_x. $\delta = 1$ nm is the grain boundary thickness, and all other variables/constants retain the same meanings previously ascribed to them. It was found that Coble creep is dominated by uranium vacancies, such that:

$$\dot{\epsilon}_{Coble} = \dot{\epsilon}_{Coble,V_U} \tag{2.6}$$

where

$$\dot{\epsilon}_{Coble} = \frac{\sigma}{G^3} \exp\left(f_{V_U,eq}\left(t\right)\right) \tag{2.7}$$

where $f_{V_U,eq}(t)$ is a polynomial of the form described by Equation 2.1, with the parameters provided in Table 2.1.

2.3 Climb-Limited Dislocation Creep

For low stresses, the movement to dislocations, which results in creep, is limited by the arrival or emission of defects that enable them to climb over an obstacle. This process occurs in the bulk lattice and can thus be described using the point defect concentrations and mobilities from the Centipede cluster dynamics simulations. In its simplest form, climb-limited creep is described by:

$$\dot{\epsilon}_{Climb} = A_1 \frac{D_x[x]\mu b}{k_B T} \left(\frac{\sigma_v}{\mu}\right)^3 \tag{2.8}$$

where A_1 is a dimensionless constant of proportionality of the order of unity (taken in this work to be exactly 1), $\mu = 75$ GPa is the shear modulus, and b is the Burgers vector (approximated by the lattice constant). $[x]$ and D_x are the irradiation-enhanced concentration and diffusivity, respectively, of defect x in the bulk lattice, as per the Centipede cluster dynamics simulations. The exponent of 3 used in this work is premised on the assumption that phenomenons such as pipe diffusion and strain-dependent absorption of defects can be omitted. This assumption will be relaxed in future work based on further atomic-scale simulations of the interactions between point defects and dislocations. All the other terms retain the same definitions previously ascribed to them. It was found that the contributions from V_U and $\{U_i : 2O_i\}$ alone could describe the climb creep rate over a wide range of temperatures, thus:

$$\dot{\epsilon}_{Climb} = \dot{\epsilon}_{Climb,V_U} + \dot{\epsilon}_{Climb,\{U_i:2O_i\}} \tag{2.9}$$

where

$$\dot{\epsilon}_{climb} = \sigma^3 \left[\exp\left(f_{\{u_i:2O_i\}}\left(t\right)\right) + \exp\left(f_{V_U}\left(t\right)\right)\right] \tag{2.10}$$

where the coefficients for the two polynomial functions ($f_{\{u_i:2O_i\}}(t)$ and $f_{V_U}(t)$) are described by Equation 2.1, as defined in Table 2.1.

Table 2.1 summarizes coefficients A–E for each of the functions in the five different creep terms. The

Table 2.1. Polynomial coefficients used in the different terms in the creep model.

Coefficient	NH $f_{\{u_i:2O_i\}}(t)$	NH $f_{V_U}(t)$	Coble $f_{V_U,eq}(t)$	Climb $f_{\{u_i:2O_i\}}(t)$	Climb $f_{V_U}(t)$
A (K^4)	0.01699251	0.10022553	0.00892327	0.01699251	0.10022553
B (K^3)	-0.3328453	-2.7922353	-0.2547609	-0.3328453	-2.7922353
C (K^2)	1.76211066	28.5246323	2.67794715	1.76211066	28.5246323
D (K)	-1.03723896	-128.748618	-16.8100963	-1.03723896	-128.748618
E (-)	-77.2703158	147.918402	-31.9439794	-86.5497859	139.7217795

units of each term are provided in the term, such that $t = 10^4/T$, where T is in K.

2.4 Combined

Figure 2.1 shows the creep rate for the various mechanisms as a function of temperature for a grain size of 10 µm and a stress of 50 MPa. At high temperatures, the Coble creep mechanism is dominant, and at low temperatures, the creep is dominated by climb creep. This highlights the importance of distinguishing among the various creep mechanisms, given that they have different grain size dependencies. In the climb-dominated regime, diffusion is governed by irradiation-enhancement processes, thus demonstrating the need to consider the various point defect diffusion mechanisms that play a role in irradiation-enhanced diffusion. The creep rate for the existing MATPRO model in BISON is included in Figure 2.1. Using this preliminary model, the creep rate (the summation of the five terms) is still many orders of magnitude below that of the existing empirical model from MATPRO. However, the MATPRO model was fit to UO_2 specimens of typical grain size and is inapplicable to the large-grained Cr_2O_3-doped UO_2. Due to the number of assumptions regarding both Coble and climb creep, this model should be treated as approximate. But by deriving this preliminary creep model, it is possible to evaluate the sensitivity of fuel performance metrics in BISON in regard to particular creep mechanisms and defects (see Section 3.2). Doing so will ensure that efforts are well targeted in ongoing and future lower length scale model development, guaranteeing maximum impact for informing engineering-scale behavior.

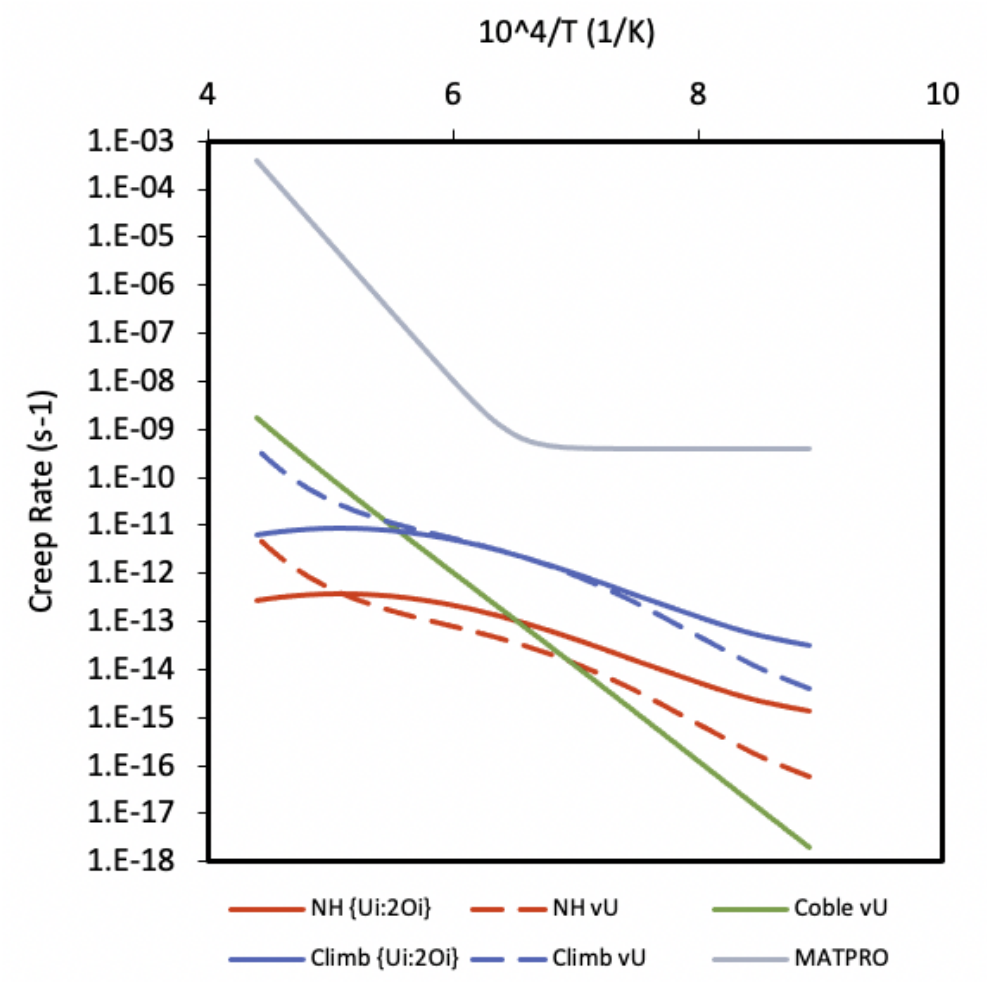

Figure 2.1. Plots of the five different creep components of the preliminary lower-length-scale-informed model, alongside the existing MATPRO model [3].

3. Application of the Creep Model

Even though the creep rate plot in Figure 2.1 shows that the preliminary multiscale modeling approach yields smaller creep rates than the existing MATPRO model, the model was applied to a normal operation simulation to see if any creep is observable in both doped and undoped UO_2. Then, given the large uncertainties in the different components of creep in the lower-length-scale-informed model, a full sensitivity analysis was conducted based on the normal operation case.

3.1 Normal Operation

A 2-D RZ 10 pellet rodlet was used as the example case to test the parameters of the creep model. Details on the rodlet are provided in Table 3.1. The main differences between the doped and undoped rods are the initial grain size and tensile strength. The previously developed fission gas release model [1] was also applied to the doped case. The creep model was applied in both cases. Given the limited range of applicability of the creep model (1123–2273 K), the linear heat generation rate (LHGR) supplied to the fuel rodlets was linearly increased from zero to 30 kW/m over 10,000 seconds. The LHGR was then held constant for ∼2.8 years (9×10^7 seconds). This LHGR gives fuel centerline temperatures near the middle of the range of applicability. However, the pellet periphery remains far below this temperature, and a check in the creep model was added so that, even if the temperature fell below 1123 K, it would still be recorded as 1123 K for the purposes of the creep calculation. If this check is absent, extreme non-physical values for the creep rate will be obtained. The tensile strength provided from AFC is used in tandem with a smeared cracking approach. Section 4 details the applicability of the different fracture models available in BISON and the results obtainable therefrom.

The results of the normal operation example case are presented in Figures 3.1, 3.2, and 3.3. The centerline temperature and the fission gas release as a function of time are presented in Figure 3.1. Due to the low creep rates predicted by the current model at these temperatures, there is no impact on the predictions. The small differences in the fuel temperatures stem from the tensile strength and the use of a smeared cracking model. The differences in fission gas release are a product of the lower length scale model that was added in previous years, as well as the large-grain doped UO_2 that reduces fission gas release.

Figures 3.2 and 3.3 show end-of-irradiation contour plots of the creep rate for each of the five different creep components; namely, Nabarro-Herring interstitials, Nabarro-Herring vacancies, Coble vacancies, climb interstitials, and climb vacancies. As expected, the creep rate values are very small. Given such small

Table 3.1. Normal-operation rodlet specifications.

	Value	Units
Number of pellets	10	-
Fuel enrichment	5	%
Pellet length	9.83	mm
Pellet outer diameter	8.2	mm
Tensile strength	83.2, 103.1 (undoped, doped)†	MPa
Radial gap width	100	µm
Clad thickness	0.56	mm
Rodlet diameter	9.52	mm
Initial fill pressure	2	MPa
Initial fill gas	Helium	-
Plenum height	26	mm
Initial fuel grain size	20, 58 (undoped, doped)	µm
Coolant inlet mass flux	3800	kg/m-s
Coolant inlet temperature	580	K
Coolant pressure	15.5	MPa

†Provided by Josh White from Los Alamos National Laboratory (LANL) as part of AFC

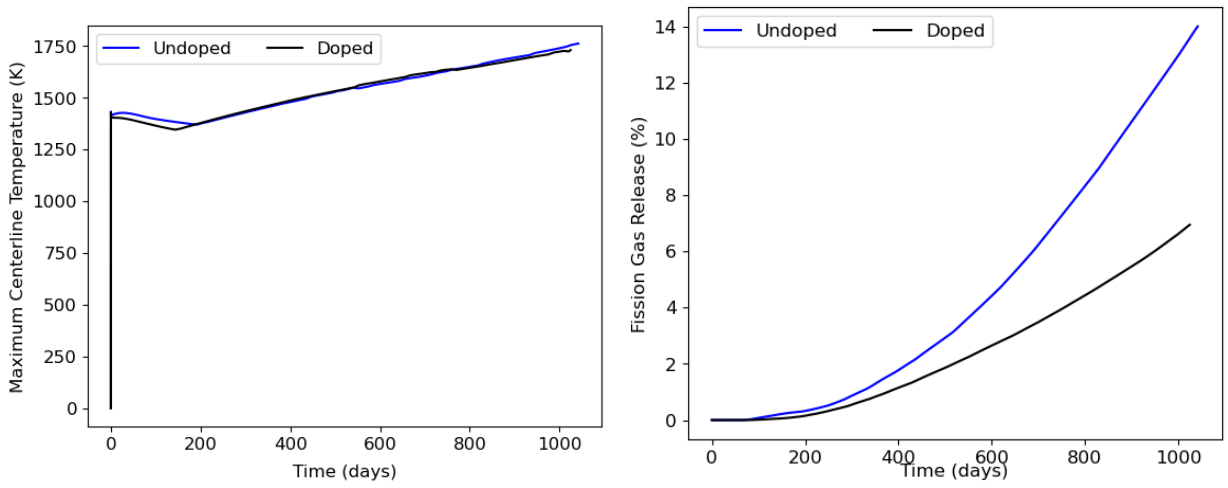

(a) (b)

Figure 3.1. Comparisons between doped and undoped UO_2 for (a) temperature and (b) fission gas release.

magnitudes, the differences within a single contour have little meaning. The main observation is that, for the terms that are dependent on grain size, (i.e., Nabarro-Herring and Coble) the doped UO_2 shows lower values than the undoped UO_2. However, doped UO_2 with higher tensile strength has larger stresses, and the stress-only dependent creep components due to climb are a bit larger in the doped UO_2 case. The striping on the plots correspond to local numerical differences in stress caused by cracking and local grain size.

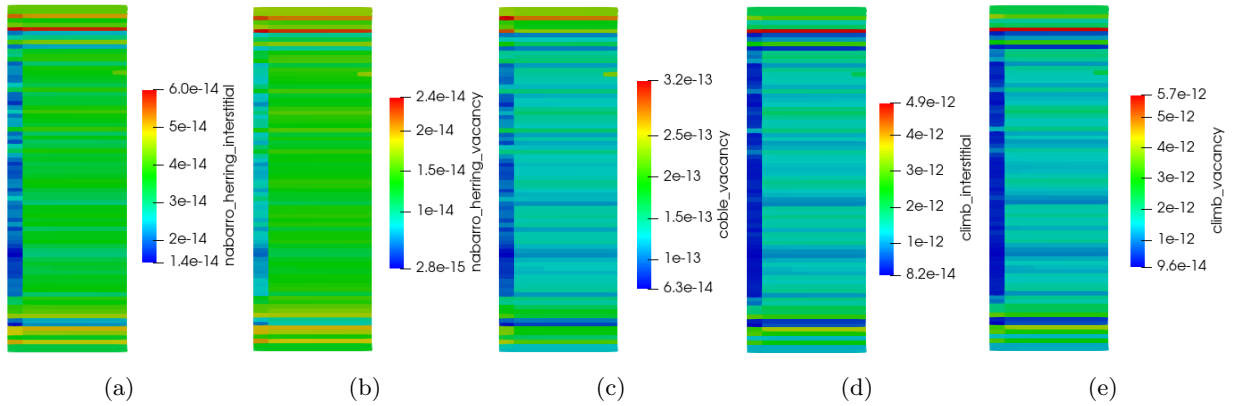

Figure 3.2. Contours for the fuel creep contributions from (a) Nabarro-Herring interstitials, (b) Nabarro-Herring vacancies, (c) Coble vacancies, (d) climb interstitials, and (e) climb vacancies for undoped fuel, using the lower-length-scale-informed creep model (scaled axially by a factor of 0.1). The cladding is not shown.

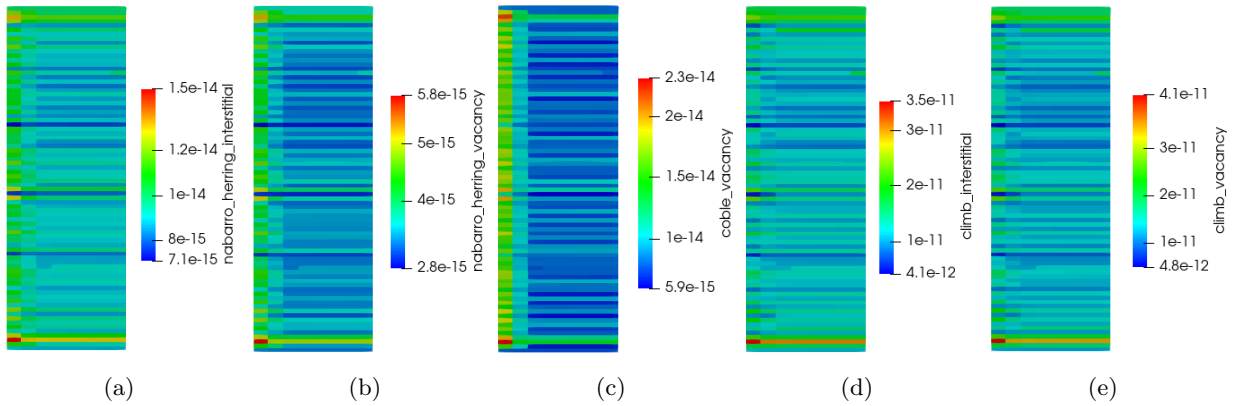

Figure 3.3. Contours for the fuel creep contributions from (a) Nabarro-Herring interstitials, (b) Nabarro-Herring vacancies, (c) Coble vacancies, (d) climb interstitials, and (e) climb vacancies for doped fuel, using the lower-length-scale-informed creep model (scaled axially by a factor of 0.1). The cladding is not shown.

3.2 Sensitivity Analysis

In presenting the creep model developed in Section 2, it was mentioned that the model is approximate and that the uncertainties are high at present. Therefore, a sensitivity analysis was performed for the normal operation case presented in Section 3.1. Table 3.2 presents the model parameters considered uncertain in this study, the parameter uncertainties, and the distributions used.

Table 3.2. Parameters varied in the sensitivity study.

Model	Uncertainty	Reference	Distribution
Young's modulus	±10%	[3]	Normal
Ultimate tensile strength	Undoped: 80.1 ± 3.1 (MPa)	AFC	Uniform
	Doped: 103.1 ± 4.6 (MPa)	AFC	Uniform
Grain size	± 20%		Normal
Nabarro-Herring interstitials	2 orders of magnitude		Loguniform
Nabarro-Herring vacancies	2 orders of magnitude		Loguniform
Coble vacancies	5 orders of magnitude		Loguniform
Climb interstitials	3 orders of magnitude		Loguniform
Climb vacancies	3 orders of magnitude		Loguniform

Figure 3.4 presents the Pearson correlation coefficients for both the doped and undoped rodlets. The Pearson correlation coefficients highlight linear relationships between inputs and outputs. The values of the coefficients are always between -1.0 and 1.0, with larger negative values indicating that, when an input value is increased, an output of interest tends to decrease. For large positive values, the output metric increases in correlation with an increase in the respective uncertain input. A relationship is typically considered significant when the absolute value of the correlation coefficient is ≥ 0.3.

The outputs of radial, axial, and hoop crack damage are a measure of fracture in the different coordinate directions, due to the smeared cracking model. It was found that, in both cases, the uncertain inputs that have the most linear correlations with the output metrics of interest are the climb contributions in the lower length scale creep model and the fuel grain size. Of the two, grain size has the greatest influence in reducing fission gas release. The correlation is stronger for the doped case because fission gases diffuse at a faster rate than undoped UO_2. The climb point defects are the dominate creep mechanism because, at the temperatures under which the fuel is operating (see Figure 3.1a), the temperature would fall in the climb-dominated regime seen in Figure 2.1. Even if the stresses in the fuel exceed the 50 MPa used to generate that plot, the climb dominance would only increase due to the stress exponent being much larger than for Nabarro-Herring and Coble creep components.

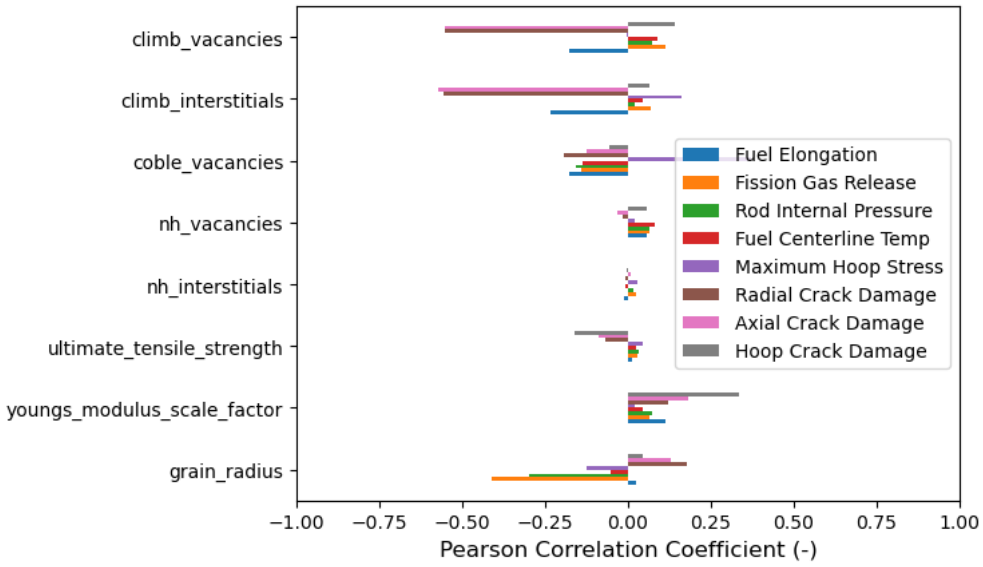

(a)

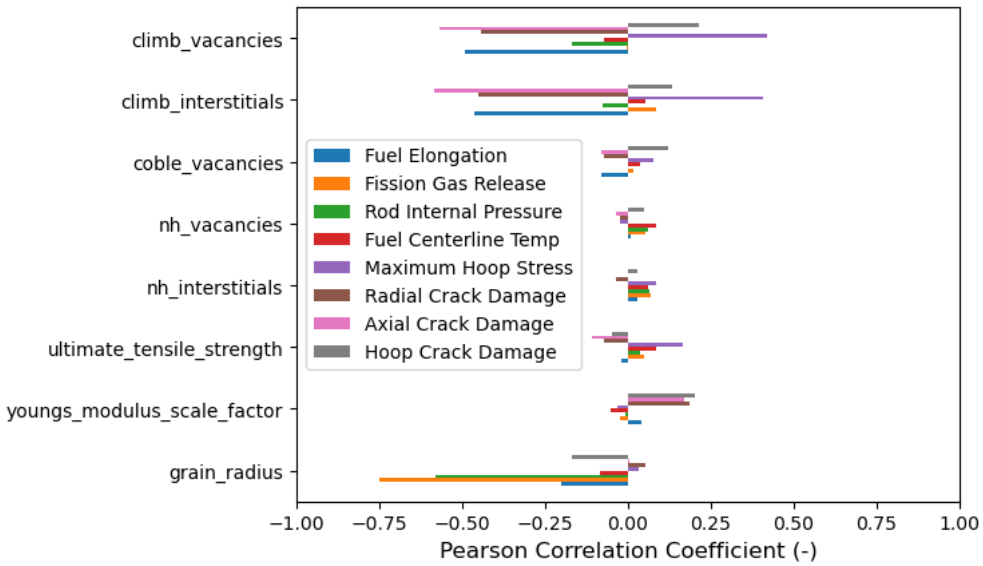

(b)

Figure 3.4. Pearson correlation coefficients between inputs and outputs of interest for (a) undoped and (b) doped UO_2.

4. Fracture Modeling

Ceramic fuel (e.g., UO_2) fractures during normal operation, due to the large thermal gradients caused by the fuel's low thermal conductivity. Adding ceramic dopants (e.g., alumina and chromia) is expected to minimally affect the thermal conductivity and specific heat properties of the material. Large temperature gradients are still expected. The difference in fracture behavior would stem from differences in the fracture toughness of the fuel, due to the larger grain size. Oguma [8] proposed the following equation for the tensile strength of UO_2:

$$\sigma_{TS} = 626.0 \exp\left(-0.057p\right) \left(0.5G + P\right)^{-0.5} \tag{4.1}$$

where p is the porosity of the fuel (%), G is the grain size (µm), and P is the pore size (µm). While Equation 4.1 is not currently implemented in BISON, it is valid for grain sizes of up to 90 µm, thus encompassing the expected range for doped UO_2 fuels. Furthermore, the model could be coupled to existing fission gas behavior models for pore size, as well as evolving density models for the current porosity within the fuel, in order to have an evolving tensile strength as irradiation progresses. This tensile strength can be used as a criterion for crack initiation when modeling fracture, as has been done by many researchers [9, 10, 11, 12, 13].

BISON offers three primary ways of incorporating the effects of fracture into an analysis: isotropic, smeared, and discrete. The applicability of each approach depends on the level of complexity and accuracy needed for the given analysis. In the isotropic case, the fuel's elastic properties (Young's modulus and Poisson's ratio) continue to degrade with the formation of each new crack. This degradation is applied uniformly throughout the fuel [14]. The degradation is not a function of grain size and would thus yield the same results for both doped and undoped UO_2.

In a smeared cracking approach to fracture (see the example in Section 3.1), the local material point becomes degraded over time once a critical stress is reached. In previous analyses, this value was the tensile strength of the fuel. The rate at which the properties degrade depends on which type of softening model is selected: abrupt, exponential, or power law. In the current analyses, the exponential softening law was used, in which the cracking is recorded in a vector material property that houses the damage in the axial, radial, and hoop directions. The crack damage in the axial, radial, and hoop directions at the end of the simulation from Section 3.1 is shown in Figure 4.1 and Figure 4.2 for the undoped and doped fuel rodlets, respectively. The crack damage is a value between 0 and 1, and is a measure of the reduced strength of the material point in the direction specified. A value of 0 indicates an intact material point, a value of 1 indicates complete

damage, and an intermediate point indicates partial damage. The results indicate that significant fracture occurs in the radial and axial directions during a hold at power without any power down. Circumferential cracking tends to form during power downs after a duration at power. Slightly less damage is observed in the doped UO_2 case, thanks to the Its higher tensile strength.

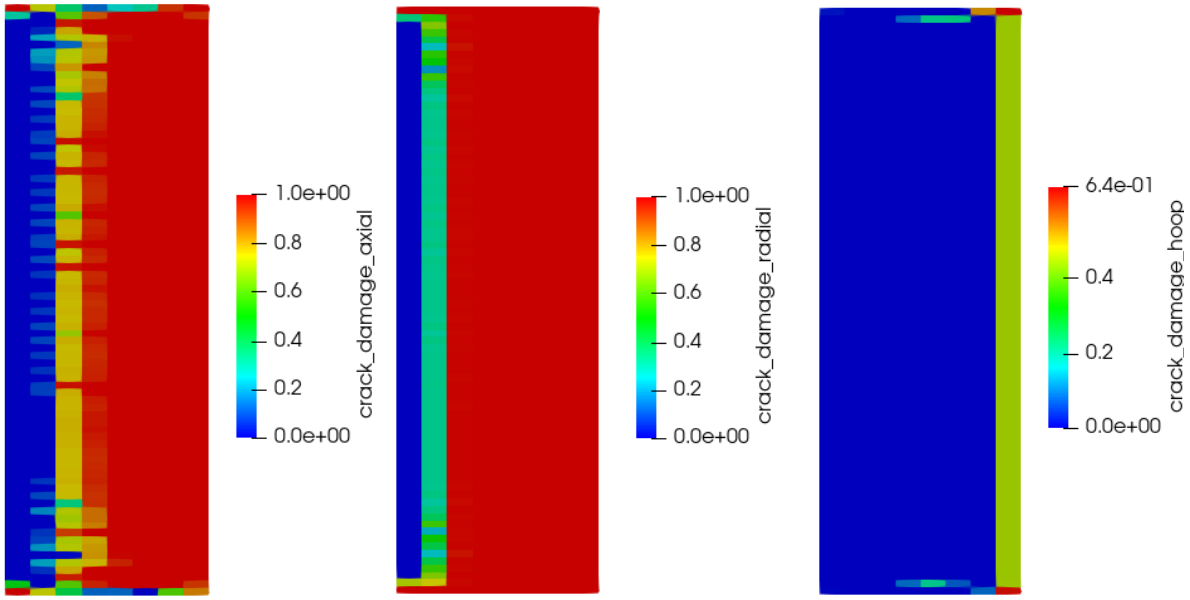

(a) (b) (c)

Figure 4.1. Contours for the (a) axial, (b) radial, and (c) hoop crack damage for the undoped UO_2 normal operation case. Scaled axially by a factor of 0.1.

The discrete approach to modeling fracture involves coupling to the extended finite element method and observing the actual fracture-related discontinuities in the mesh [10, 13]. At present, the discrete approach is limited to modeling radial crack formation, and is typically done on a cross-sectional slice—or multiple cross-sectional slices stacked along the axial direction of the fuel rod. The tensile strengths provided from AFC feature very limited uncertainty (see Table 3.2) even though the tensile strength of UO_2 can vary from 80 to 150 MPa, depending on the microstructural features and manufacturing processes [15]. Gamble et al. [13] investigated the effect of tensile strength uncertainty on predictions regarding the number of cracks that form during irradiation. The ranges evaluated exceeded the values of both AFC measurements, and there was found to be high uncertainty in the number of radial cracks that form, due to randomization of the tensile strength. Additional work is necessary to investigate the influence of a time-dependent tensile strength as a function of grain size, pore size, and porosity, as described by Equation 4.1.

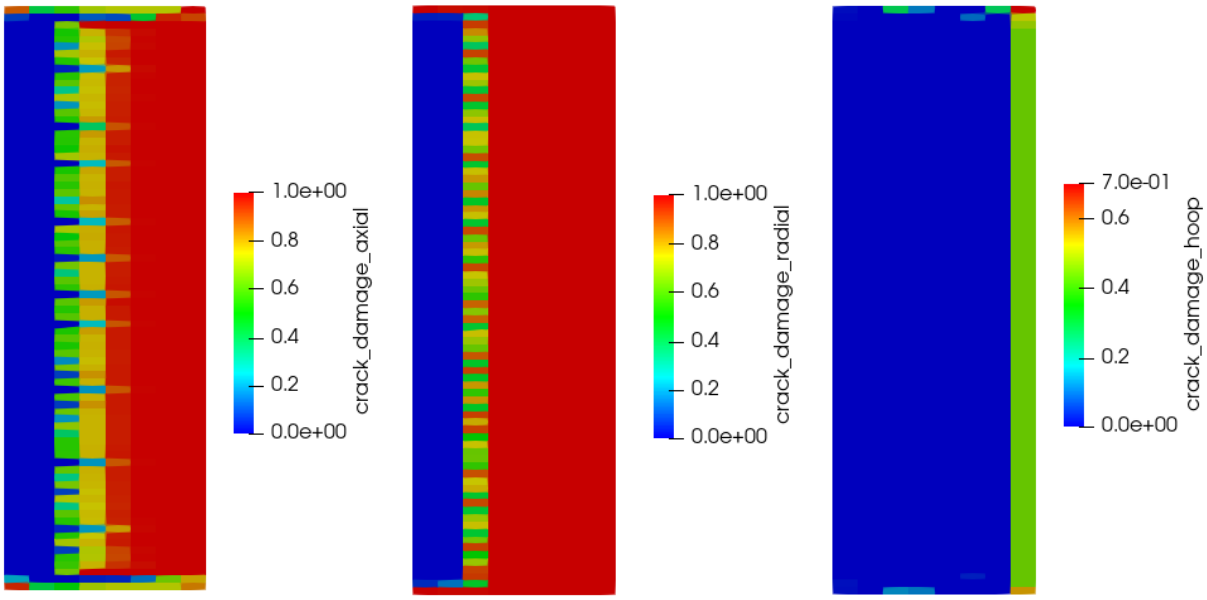

(a) (b) (c)

Figure 4.2. Contours for the (a) axial, (b) radial, and (c) hoop crack damage for the Cr_2O_3-doped UO_2 normal operation case. Scaled axially by a factor of 0.1.

5. Validation Case Improvements

Over the years, Cr_2O_3-doped UO_2 modeling has primarily focused on fission gas release. In support of validating those efforts, simulations of three experiments from the Halden reactor were added to the BISON validation suite in order to document impacts from new models as they become available [16]. Those cases are IFA-677.1 rods 1 and 5 [17, 18, 19] and IFA-716 rod 1 [20, 21, 22]. Each year, the temperature validation predictions for the IFA-677.1 rods have significantly overpredicted the temperatures at the upper and lower thermocouples during the second half of irradiation (see [16] for details). This year, the input power provided by Halden was modified based on various recommendations [23]. Two corrections were made. The first resulted in changes to the axial profile, with a reduction in power at the bottom (1.5%) and top (3.5%) power nodes, a slight increase at the upper and lower thermocouple (2.6%) locations, and a larger increase at the middle power node (4.3%). The second was an approximate 2% reduction in the average linear power after approximately 14.5 MWd/kgU and lasting until the end of the irradiation, due to changes in the reactor environment near the IFA-677 test rig. This 2% change was determined via neutronics calculations, and [23] mentions that this change is likely insufficient to completely negate the power discrepancy seen during the later stages of irradiation. Nevertheless, both changes were applied to IFA-677.1 rods 1 and 5. Details on the rod and power history can be found in [16], along with the results of previous analyses. Here, the best estimate fission gas release model informed by lower-length scale calculations is used, corresponding to `cr_doped_option = 5` in the `Sifgrs` fission gas release model in BISON.

For IFA-677.1 rod 1, the calculated and measured fuel centerline temperature evolutions at the upper and lower thermocouple positions are compared in Figures 5.1a and 5.1b, respectively.

For both positions, the BISON calculation underpredicts the measurements by ∼100 K. The differences between the model predictions and the experiment are minimal for the fourth and fifth cycles. For the sixth cycle, overprediction of up to ∼200 K is observed—an improvement on the previously presented results found in [16]. Therefore, the power correction has some influence on the temperature predictions but is insufficient to account for the entire discrepancy.

The calculated fission gas release as a function of rod average burnup is shown in Figure 5.2, along with the measured data (which are inferred from the online measurement of inner rod pressure [18]). BISON predicts a value of ∼11%, as compared to the experimental 22%. This is within a factor of 2 and is considered adequate, given the uncertainties associated with fission gas release modeling [24].

In Figure 5.3, the time evolution of the rod inner pressure, as calculated by BISON, is compared to the

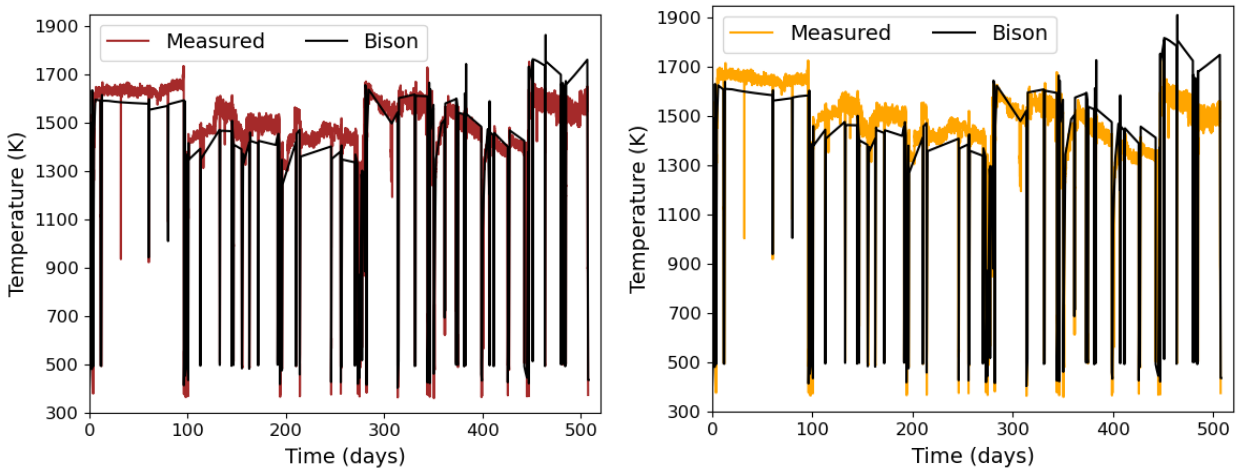

(a) (b)

Figure 5.1. Comparison of predicted and measured fuel centerline temperature histories at the (a) upper and (b) lower thermocouple locations for IFA-677.1 rod 1.

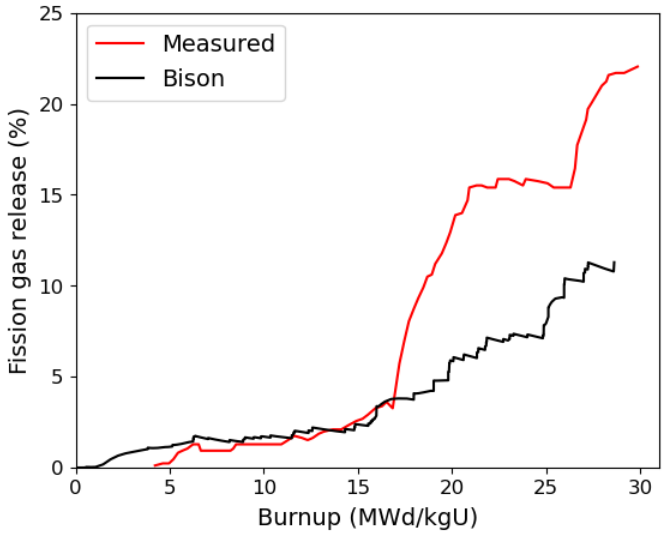

Figure 5.2. Comparison of predicted and measured fission gas release as a function of rod average burnup for IFA-677.1 rod 1.

online experimental data from the pressure transducer. Overall, the prediction appears reasonably accurate, though a moderate overprediction of the measured rod inner pressure is observed in the final three cycles. The discrepancies are partly due to inaccuracies in calculating the plenum temperature.

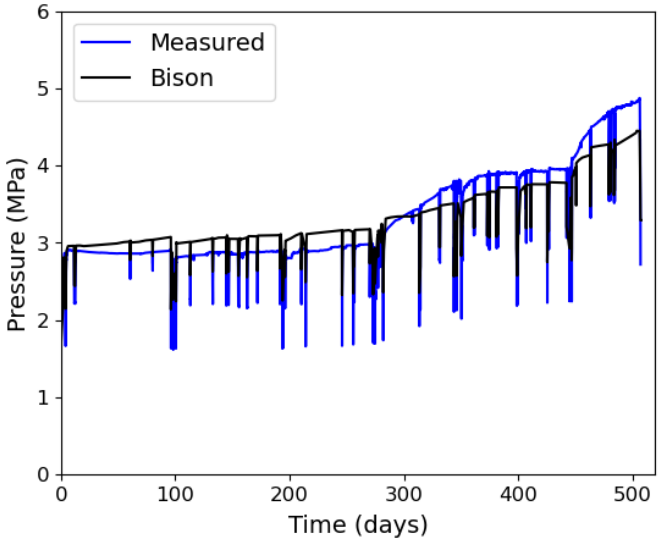

Figure 5.3. Comparison of predicted and measured inner rod pressure histories for IFA-677.1 rod 1.

6. Conclusions

The pursuit of doped-UO_2 fuels for use in LWRs has accelerated the application of multiscale modeling approaches in order to support accelerated qualification by enabling an enhanced understanding of the performance of these fuels. These modeling approaches explore regions outside the range of applicability of the current empirical models. This report focuses on the preliminary development of a creep model that is applicable to both doped and undoped UO_2. The model's current status was presented, then the model was applied to a 10-pellet rodlet, with sensitivity analysis included. It was found that higher-tensile-strength Cr_2O_3-doped UO_2 coupled with a smeared cracking model yielded a minor centerline temperature reduction early in the life of the fuel. As in previous work, fission gas release was found to be less than undoped UO_2. Sensitivity analysis indicated that the climb creep mechanisms were the overall dominate creep mechanism, with individual point defects being of roughly equal importance. Grain size was also deemed important, particularly for fission gas release. Finally, the modifications to the provided input power for the IFA-677 Cr_2O_3-doped UO_2 validation cases yielded improvements in BISON predictions for the later cycles of irradiation.

7. Future work

The work presented in this report gave an overview of the development and evaluation of a preliminary creep model applicable to UO_2 and large-grain doped UO_2. The form of the equations, presented as the exponential of polynomials, is atypical of creep correlations used in fuel performance analysis. The sensitivity analysis completed in this work highlighted the important mechanisms of creep that must be further understood, particularly dislocation climb and Coble. This requires additional lower length scale investigations. Once these calculations are complete, a more refined engineering-scale model will be added to BISON. Reevaluation of the validation cases discussed in Section 5 would then reveal further improvements.

Regarding the validation of doped UO_2 fuel in BISON, the total number of cases against which to compare is three. The IFA-677.1 series, for which two rods were analyzed, contains another four rods, all of which could be added. The IFA-716.1 series, in which a single rod was analyzed, contains another five rods, all of which could be added. Finally, a newer Halden test series, identified as IFA-720.3, also contains doped UO_2 specimens that could provide additional cases against which to test new model developments. Future work includes adding (at minimum) a subset of these cases.

8. Publications

This report highlights advancements in the development of a multiscale modeling and AFC/NEAMS collaboration on the mechanical properties of Cr_2O_3-doped UO_2. However, it is important to highlight other accident-tolerant fuel (ATF)-related efforts that resulted in publications based on NEAMS work in previous years. More specifically, work on U_3Si_2 fuel has concluded and was published in the following two journal articles:

1. M.W.D. Cooper, K.A. Gamble, L. Capolungo, C. Matthews, D.A. Andersson, B. Beeler, C.R. Stanek, K. Metzger, Irradiation-enhanced diffusion and diffusion-limited creep in U_3Si_2, Journal of Nuclear Materials, 555, 2021, 153129, https://doi.org/10.1016/j.jnucmat.2021.153129.
2. K.A. Gamble, G. Pastore, M.W.D. Cooper, D.A. Andersson, C. Matthews, B. Beeler, L.K. Aagesen, T. Barani, D. Pizzocri, Improvement of the BISON U_3Si_2 modeling capabilities based on multiscale developments to modeling fission gas behavior, Journal of Nuclear Materials, 555, 2021, 153097, https://doi.org/10.1016/j.jnucmat.2021.153097.

Bibliography

[1] M. W. D. Cooper et al. "Fission gas diffusion and release for Cr_2O_3-doped UO_2: From the atomic to the engineering scale". In: *Journal of Nuclear Materials* 545 (2021), p. 152590. DOI: https://doi.org/10.1016/j.jnucmat.2020.152590.

[2] R. L. Williamson et al. "BISON: A Flexible Code for Advanced Simulation of the Performance of Multiple Nuclear Fuel Forms". In: *Nuclear Technology* 207.7 (2021), pp. 954–980. DOI: 10.1080/00295450.2020.1836940.

[3] D. L. Hagrman and G. A. Reymann. "MATPRO-Version 11: a handbook of materials properties for use in the analysis of light water reactor fuel rod behavior". In: (Feb. 1979). DOI: 10.2172/6442256. URL: https://www.osti.gov/biblio/6442256.

[4] C. Matthews et al. "Cluster dynamics simulation of uranium self-diffusion during irradiation in UO_2". In: *Journal of Nuclear Materials* 527 (2019), p. 151787. DOI: https://doi.org/10.1016/j.jnucmat.2019.151787.

[5] F. R. N. Nabarro. "Deformation of Crystals by the Motion of Single Ions in Report of a Conference on the Strength of Solids (Bristol, U.K.)" In: *Physical Society London* (1948), pp. 75–90.

[6] C. Herring. "Diffusional Viscosity of a Polycrystalline Solid". In: *Journal of Applied Physics* 21 (5 1948), pp. 437–445. DOI: https://doi.org/10.1063/1.1699681.

[7] R. L. Coble. "A Model for Boundary Diffusion Controlled Creep in Polycrystalline Materials". In: *Journal of Applied Physics* 34 (1963), pp. 1679–1682. DOI: https://doi.org/10.1063/1.1702656.

[8] M. Oguma. "Microstructure Effects on Fracture Strength of UO_2 Fuel Pellets". In: *Journal of Nuclear Science and Technology* 19.12 (1982), pp. 1005–1014. DOI: https://doi.org/10.1080/18811248.1982.9734249.

[9] H. Huang, B. Spencer, and J. Hales. "Discrete element method for simulation of early-life thermal fracturing behavior in ceramic nuclear fuel pellets". In: *Nuclear Engineering and Design* 278 (2014), pp. 515–528.

[10] B. W. Spencer et al. "Discrete modeling of early-life thermal fracture in ceramic nuclear fuel". In: *Proceedings of WRFPM2014*. https://www.osti.gov/biblio/1177218. 2014.

[11] W. Jiang, B. W. Spencer, and J. E. Dolbow. "Ceramic nuclear fuel fracture modeling with the extended finite element method". In: *Engineering Fracture Mechanics* 223 (Jan. 2020), p. 106713.

[12] J. Sercombe, I. Aubrun, and C. Nonon. "Power ramped cladding stresses and strains in 3D simulations with burnup-dependent pellet-clad friction". In: *Nuclear Engineering and Design* 242 (2012), pp. 164–181.

[13] K.A. Gamble et al. "Mechanistic verification of empirical UO_2 fuel fracture models". In: *Journal of Nuclear Materials* 556 (2021), p. 153163. ISSN: 0022-3115. DOI: 10.1016/j.jnucmat.2021.153163. URL: https://www.sciencedirect.com/science/article/pii/S002231152100386X.

[14] T. Barani et al. "Isotropic softening model for fuel cracking in BISON". In: *Nuclear Engineering and Design* 342 (2019), pp. 257–263.

[15] M. Oguma. "Cracking and Relocation behavior of Nuclear Fuel Pellets during Rise to Power". In: *Nuclear Engineering and Design* 76 (1983), pp. 35–45. DOI: https://doi.org/10.1016/0029-5493(83)90045-6.

[16] K. A. Gamble et al. *ATF material model development and validation for priority fuel concepts*. Tech. rep. CASL-U-2019-1870-000 Rev.0. Idaho National Laboratory, 2019.

[17] B. Thérache. *The High Initial Rating Test, IFA-677.1: Results after First Cycle of Irradiation*. Tech. rep. HWR-819. OECD Halden Reactor Project, 2005.

[18] R. Jošek. *The High Initial Rating Test IFA-677: Final Report on In-Pile Results*. Tech. rep. HWR-872. OECD Halden Reactor Project, 2008.

[19] H. K. Jenssen. *PIE Report on Six UO_2 Fuel Rods Irradiated in IFA-677 High Initial Rating Test*. Tech. rep. HWR-968. OECD Halden Reactor Project, 2010.

[20] O. Brémont. *IFA-716.1 Fission gas release mechanisms*. Tech. rep. HWR-1008. OECD Halden Reactor Project, 2011.

[21] T. Tverberg. *Update on the in-pile results from the fission gas release mechanisms study in IFA-716*. Tech. rep. HWR-1090. OECD Halden Reactor Project, 2014.

[22] B. Baurens. *In-pile results from the fission gas release mechanisms study in IFA-716 after final unloading*. Tech. rep. HWR-1161. OECD Halden Reactor Project, 2016.

[23] W. Weisenak. *Modifications to IFA-677 data conversion*. Tech. rep. HWR-1263. OECD Halden Reactor Project, 2019.

[24] G. Pastore et al. "Uncertainty and sensitivity analysis of fission gas behavior in engineering-scale fuel modeling". In: *Journal of Nuclear Materials* 465 (2015), pp. 398–408. DOI: https://doi.org/10.1016/j.jnucmat.2014.09.077.